Geophys. J. Int. (1992) **109**, 363–375

Geodetic data inversion using a Bayesian information criterion for spatial distribution of fault slip

T. Yabuki* and M. Matsu'ura

Department of Earth and Planetary Physics, Faculty of Science, The University of Tokyo, Tokyo 113, *Japan*

Accepted 1991 November 12. Received 1991 November 11; in original form 1991 September 17

SUMMARY

We developed a new inversion method to reconstruct static images of seismic sources from geodetic data, using Akaike's Bayesian Information Criterion (ABIC). Coseismic surface displacements are generally related with a slip distribution on a fault surface by linear integral equations. Parametric expansion of the fault slip distribution by a finite number of known basis functions yields a set of observation equations expressed in a simple vector form. Incorporating prior constraints on the smoothness of slip distribution with the observation equations, we construct a Bayesian model with unknown hyperparameters. The optimal values of the hyperparameters, which control the structure of the Bayesian model, are objectively determined from observed data by using ABIC. Once the values of hyperparameters are determined, we can use the maximum likelihood method to find the optimal distribution of fault slip. We examined the validity of this method through a numerical experiment using theoretical data with random noise. We analysed geodetic data associated with the 1946 Nankaido earthquake ($M_s = 8.2$) by using this method. The result shows that the fault slip distribution of this earthquake has two main peaks of 4 and 6 m, located off Kii Peninsula and Muroto Promontory. These two high-slip areas are clearly separated by a low-slip zone extending along Kii Strait. Such a slip distribution corresponds with the fact that the rupture process of this earthquake in the western part is notably different from that in the eastern part.

Key words: ABIC, Bayesian modelling, fault slip distribution, geodetic data.

1 INTRODUCTION

The occurrence of a large shallow earthquake brings about notable surface displacements in and around the focal area. The coseismic surface displacements are obtained from the comparison of pre- and post-seismic geodetic measurements. The representation theorem in elastodynamics relates the surface displacements with a slip distribution on a fault surface by linear integral equations. Therefore we can set up the inverse problem of reconstructing the static image of a seismic source from observed geodetic data.

The problems of geodetic data inversion may be divided into two classes according to whether the geometry of a fault surface is known or not. When the fault geometry is unknown, which is the case of most intraplate earthquakes, the problem is essentially non-linear. This class of problems has been treated in a series of papers by Matsu'ura and his co-workers (Matsu'ura 1977a, b; Matsu'ura *et al.* 1980; Matsu'ura & Hasegawa 1987). When the fault geometry is known, which is the case of large earthquakes occurring at plate boundaries, the problem becomes linear. In the present study we treat only this class of problems.

In the second class of problems the unknown is the spatial distribution of slip vectors on a given fault surface. We usually divide the fault surface into a number of fault patches and take the dip-slip and strike-slip components on each fault patch as unknown parameters. Furthermore, if the directions of slip vectors are known, the problem becomes much simpler; the unknown is only the magnitude of slip vectors. Miyashita & Matsu'ura (1978), Ward & Barrientos (1986), and Barrientos (1988) have treated such a special case.

To obtain a clear image of a seismic source, in general, we must take the number of fault patches, and hence the number of model parameters, as large as possible. However, the increase of the number of model parameters amplifies estimation errors and leads to instability in the solution,

* Present address: Hydrographic Department, Maritime Safety Agency, Tokyo 104, Japan.

because observed data are always inaccurate and insufficient. As pointed out by Backus & Gilbert (1970), the essential problem in geophysical data inversion is to compromise these reciprocal requirements for model resolution and estimation errors in a natural way. In the formalism of linear inversion, Jackson (1979) demonstrated that the explicit use of prior information about model parameters enables us to naturally resolve this essential problem. Jackson's approach for linear inversion was soon extended to non-linear cases by Tarantola & Valette (1982a, b), Jackson & Matsu'ura (1985), and Matsu'ura & Hasegawa (1987) on the basis of probability theory.

The prior information available for the present problem comes from several different sources. From seismological observations, for example, we may obtain some prior information about the extent of a faulting region and the average magnitude and direction of slip vectors. This sort of prior information can be treated in the same way as observed data, since the degree of its uncertainty is fairly definite. Another sort of prior information comes from physical consideration for earthquake rupture; that is, the spatial variation of fault slip must be smooth in some degree because of the finiteness in the fracture strength of actual rocks. In the classical inversion methods this sort of prior information has been used in an implicit way to judge whether or not the inverted result is physically reasonable.

In the present study, we combine the prior information about the smoothness of fault slip distribution with the information coming from observed data by using Bayes' theorem, and construct a highly flexible model with hyperparameters, called a Bayesian model. The Bayesian model consists of a family of parametric models; that is, different values of hyperparameters give different parametric models. The selection of a specific model from among the family of parametric models can be objectively done by using a Bayesian information criterion (ABIC) proposed by Akaike (1980) on the basis of the entropy maximization principle (Akaike 1977). Once a specific parametric model is selected, we can use the maximum likelihood method to determine the optimum values of model parameters.

In Section 2 we formulate the problem and develop a new method of geodetic data inversion. The validity of this inversion method is examined through a numerical experiment in Section 3. To demonstrate the applicability of our method to actual cases, we analyse the geodetic data associated with the 1946 Nankaido earthquake in Section 4.

2 MATHEMATICAL FORMULATION

2.1 Representation of surface displacements

We consider a discontinuity in tangential displacement, $\Delta\mathbf{u}(\xi)$, across a fault surface S embedded in a homogeneous, isotropic, elastic half-space ($x_3 \leq 0$) as shown in Fig. 1. According to the representation theorem in elastodynamics (Maruyama 1963; Burridge & Knopoff 1964; Backus & Mulcaphy 1976a, b), the static surface displacements $u_i(\mathbf{x})$ caused by the displacement discontinuity can be

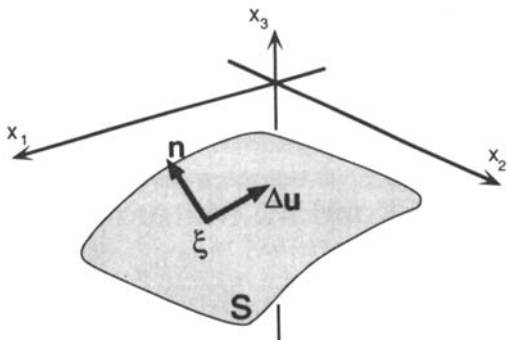

Figure 1. A schematic diagram showing the system of coordinates and the geometry of a fault surface. S indicates a fault surface embedded in the elastic half-space ($x_3 \leq 0$). $\mathbf{n}$ is a unit normal to S and $\Delta\mathbf{u}$ is a slip vector on S.

expressed in the following integral form:

$$u_i(\mathbf{x}) = \sum_{p=1}^{3}\sum_{q=1}^{3}\int_S G_{ip,q}(\mathbf{x}, \xi) m_{pq}(\xi)\, dS(\xi) \qquad (i = 1, 2, 3), \tag{1}$$

with

$$m_{pq}(\xi) = \mu[n_p(\xi)\Delta u_q(\xi) + n_q(\xi)\Delta u_p(\xi)] \qquad (p, q = 1, 2, 3), \tag{2}$$

where $G_{ip,q}(\mathbf{x}, \xi)$ is the derivative of Green's tensor $G_{ip}(\mathbf{x}, \xi)$ with respect to ξ_q, $m_{pq}(\xi)$ the moment tensor density localized on the fault surface S, μ the rigidity of the medium, and $n_j(\xi)$ the j component of a unit normal to the fault surface. The analytical expressions of $G_{ip,q}$, which were first obtained by Maruyama (1964), are given in Appendix A.

We may define the fault surface $S(\xi)$ by

$$\xi_3 = f(\xi_1, \xi_2) \tag{3}$$

in the case of low-angle faults. Then the components of the unit normal vector $\mathbf{n}$ are given by

$$\begin{aligned} n_1 &= -f_1/\sqrt{1+f_1^2+f_2^2}, \\ n_2 &= -f_2/\sqrt{1+f_1^2+f_2^2}, \\ n_3 &= 1/\sqrt{1+f_1^2+f_2^2}, \end{aligned} \tag{4}$$

with

$$f_j = \frac{\partial f}{\partial \xi_j} \qquad (j = 1, 2). \tag{5}$$

Once the geometry of a fault surface is given, the three components of the slip vector $\Delta\mathbf{u}$ are no longer independent of one another. The components of the slip vector must satisfy the following condition:

$$\sum_{j=1}^{3} n_j \Delta u_j = -f_1\Delta u_1 - f_2\Delta u_2 + \Delta u_3 = 0 \tag{6}$$

or, choosing Δu_1 and Δu_2 as independent variables,

$$\Delta u_3 = f_1\Delta u_1 + f_2\Delta u_2. \tag{7}$$

Then we may rewrite the expression for the static surface

displacements as

$$u_i = \mu \sum_{j=1}^{2} \sum_{r=1}^{3} \int_S [(G_{ij,r} + G_{ir,j}) + f_j(G_{i3,r} + G_{ir,3})](n_r/n_3)\Delta u_j \, d\xi_1 \, d\xi_2. \quad (8)$$

Our problem is to estimate the spatial distributions of $\Delta u_1(\xi_1, \xi_2)$ and $\Delta u_2(\xi_1, \xi_2)$ from observed surface displacement data. The distribution of the remaining slip component, $\Delta u_3(\xi_1, \xi_2)$, can be directly reconstructed from Δu_1 and Δu_2 by using equation (7).

2.2 Parametric expansion of slip distribution

We represent the spatial distribution of each slip component by linear combination of a finite number (KL) of basis functions Φ_{kl} defined on the ξ_1–ξ_2 plane as

$$\Delta u_j(\xi_1, \xi_2) = \sum_{k=1}^{K} \sum_{l=1}^{L} a_{jkl}\Phi_{kl}(\xi_1, \xi_2) \qquad (j = 1, 2). \quad (9)$$

Substituting this expression into equation (8), and carrying out the integration with respect to ξ_1 and ξ_2, we obtain the following relation:

$$u_i = \sum_{j=1}^{2} \sum_{k=1}^{K} \sum_{l=1}^{L} H_{ijkl}a_{jkl} \qquad (i = 1, 2, 3), \quad (10)$$

with

$$H_{ijkl} = \mu \sum_{r=1}^{3} \int_S [(G_{ij,r} + G_{ir,j}) + f_j(G_{i3,r} + G_{ir,3})](n_r/n_3)\Phi_{kl} \, d\xi_1 \, d\xi_2. \quad (11)$$

For a given point on the surface of the semi-infinite medium we can evaluate the above integral straightforwardly. Then our problem can be reduced to the problem of determining the values of the expansion coefficients a_{jkl} ($j = 1, 2$; $k = 1, \ldots, K$; $l = 1, \ldots, L$) from observed data. Once the values of a_{jkl} are determined, we can reconstruct the spatial distribution of each slip component by using equation (9).

As the basis functions we choose the normalized bicubic B-splines defined by

$$\Phi_{kl}(\xi_1, \xi_2) = N_k(\xi_1)N_l(\xi_2) \qquad (k = 1, \ldots, K; l = 1, \ldots, L), \quad (12)$$

where

$$N_j(s) = 4\Delta s M_{4,j+2}(s), \quad (13)$$

and $M_{4,j}(s)$ is the B-spline function of order 4 (degree 3) with an equally spaced local support ($s_j - 4\Delta s \le s < s_j$), defined by the following de Boor–Cox recurrence formula (de Boor 1972; Cox 1972):

$$M_{r,j}(s) = \frac{1}{r\Delta s}\{[s - s_j + (j - r)\Delta s]M_{r-1,j-1}(s) + (s_j - s)M_{r-1,j}(s)\} \quad (14)$$

with

$$M_{1,j}(s) = \begin{cases} 1/\Delta s & (s_j - \Delta s \le s < s_j), \\ 0 & (s < s_j - \Delta s, \; s_j \le s). \end{cases} \quad (15)$$

Concrete expressions for $M_{4,j}(s)$ are given in Appendix B.

The normalized bicubic B-spline $\Phi_{kl}(\xi_1, \xi_2)$ has a bell shape and takes the maximum value of 1.0 at the (k, l) knot point on the ξ_1–ξ_2 plane. Fig. 2 gives the graphic representation of $\Phi_{kl}(\xi_1, \xi_2)$.

2.3 Observation equations

Let $u_i(\mathbf{x}_p)$ be the observed value of the vertical ($i = 3$) or horizontal ($i = 1$ or 2) component of coseismic surface displacement at $\mathbf{x} = \mathbf{x}_p$. Then, using the theoretical relation (10), we may write observation equations as

$$u_i(\mathbf{x}_p) = \sum_{j=1}^{2} \sum_{k=1}^{K} \sum_{l=1}^{L} H_{ijkl}(\mathbf{x}_p)a_{jkl} + e_{ip}, \quad (16)$$

where e_{ip} denote random errors, consisting of measurement errors and modelling errors.

Now we rearrange the observed data $u_i(\mathbf{x}_p)$, the random errors e_{ip}, and the expansion coefficients a_{jkl} in some order, respectively, and define a data vector $\mathbf{d}$, an error vector $\mathbf{e}$, and a model parameter vector $\mathbf{a}$ as

$$\mathbf{d}^T = [u_1(\mathbf{x}_1), u_1(\mathbf{x}_2), \ldots, u_1(\mathbf{x}_{N_1}); u_2(\mathbf{x}_1), u_2(\mathbf{x}_2), \ldots, u_2(\mathbf{x}_{N_1}); u_3(\mathbf{x}_{N_1+1}), u_3(\mathbf{x}_{N_1+2}), \ldots, u_3(\mathbf{x}_{N_1+N_2})], \quad (17)$$

$$\mathbf{e}^T = [e_{11}, e_{12}, \ldots, e_{1N_1}; e_{21}, e_{22}, \ldots, e_{2N_1}; e_{3N_1+1}, e_{3N_1+2}, \ldots, e_{3N_1+N_2}], \quad (18)$$

$$\mathbf{a}^T = [a_{111}, a_{112}, \ldots, a_{11L}; \ldots; a_{1K1}, a_{1K2}, \ldots, a_{1KL}; a_{211}, a_{212}, \ldots, a_{21L}; \ldots; a_{2K1}, a_{2K2}, \ldots, a_{2KL}]. \quad (19)$$

Then the observation equation (16) can be rewritten in the

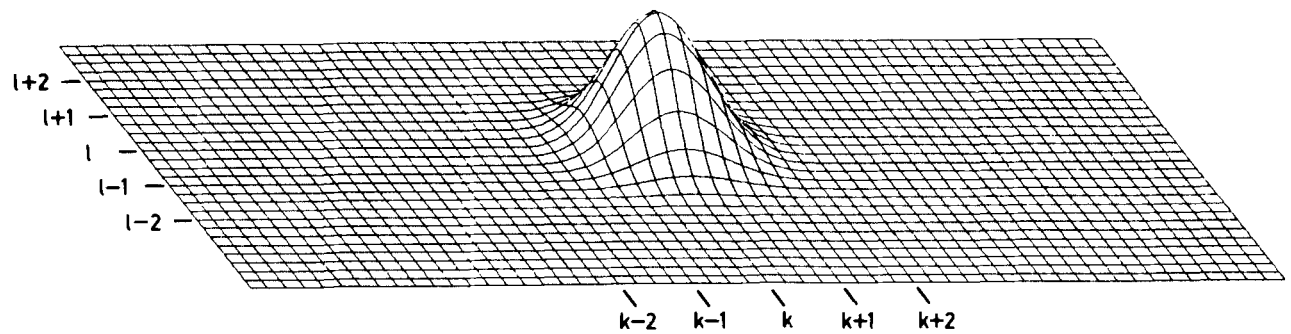

Figure 2. Graphic representation of a bicubic B-spline function Φ_{kl}.

following simple vector form:

$$\mathbf{d} = \mathbf{H}\mathbf{a} + \mathbf{e} \tag{20}$$

where $\mathbf{H}$ is a $N(=2N_1 + N_2) \times M(=2KL)$ dimensional coefficient matrix, whose IJ element is defined by

$$H_{IJ} = H_{ijkl}(\mathbf{x}_p) \tag{21}$$

with

$$I = \begin{cases} (i-1)N_1 + p & \text{if } i = 1 \text{ or } 2, \\ (i-1)N_1 + (p - N_1) & \text{if } i = 3, \end{cases} \tag{22}$$

and

$$J = (j-1)KL + (k-1)L + l. \tag{23}$$

The observation equation (20) contains the random errors $\mathbf{e}$, which generally consist of measurement errors and modelling errors. The modelling errors come from deficiency in theoretical modelling, and so depend on the number of basis functions used for the parametric expansion. For simplicity we assume the errors $\mathbf{e}$ to be Gaussian, with zero mean and covariance $\sigma^2\mathbf{E}$:

$$\mathbf{e} \sim N(\mathbf{0}, \sigma^2\mathbf{E}) \tag{24}$$

where σ^2 is an unknown scale factor for the covariance of $\mathbf{e}$. This assumption will be justified when the modelling errors are much smaller than the measurement errors. Then, from equations (20) and (24), we have a stochastic model which relates the data $\mathbf{d}$ with the model parameters $\mathbf{a}$ as

$$p(\mathbf{d} \mid \mathbf{a}; \sigma^2) = (2\pi\sigma^2)^{-N/2} \|\mathbf{E}\|^{-1/2} \times \exp\left[-\frac{1}{2\sigma^2}(\mathbf{d} - \mathbf{H}\mathbf{a})^{\mathrm{T}}\mathbf{E}^{-1}(\mathbf{d} - \mathbf{H}\mathbf{a})\right]. \tag{25}$$

Here $\|\mathbf{E}\|$ denotes the absolute value of the determinant of $\mathbf{E}$. Given the data $\mathbf{d}$, we may regard $p(\mathbf{d} \mid \mathbf{a}; \sigma^2)$ as a function of $\mathbf{a}$ and σ^2. When so regarded, following Fisher (1922), we call it the likelihood function of $\mathbf{a}$ and σ^2 for given $\mathbf{d}$, and use it as a basic device for the extraction of the information supplied by the data.

2.4 Prior constraints

It is now widely accepted that the source of earthquakes is brittle shear fracture occurring in the earth's interior. Since the fracture strength of rocks is finite, the stress field in and around the faulting region is also finite. The finiteness in stress requires the smooth variation of slip along the fault surface. This is a kind of prior information about the fault slip distribution.

As a measure of the roughness of fault slip distribution we introduce the following quantity:

$$r = \sum_{j=1}^{2} \int_S \frac{1}{n_3}\left[\left(\frac{1}{h_1^2}\frac{\partial^2 \Delta u_j}{\partial \xi_1^2}\right)^2 + 2\left(\frac{1}{h_1 h_2}\frac{\partial^2 \Delta u_j}{\partial \xi_1 \partial \xi_2}\right)^2 + \left(\frac{1}{h_2^2}\frac{\partial^2 \Delta u_j}{\partial \xi_2^2}\right)^2\right] d\xi_1 \, d\xi_2, \tag{26}$$

with

$$h_i = \sqrt{1 + f_i} \qquad (i = 1, 2). \tag{27}$$

Here n_3 and f_i $(i = 1, 2)$ are the ξ-dependent variables defined in equations (4) and (5). For simplicity we consider the case in which the distortion of the fault surface is not so strong. In such a case we may replace h_1, h_2, and n_3 in (26) with their spatial averages, $\bar{h}_1$, $\bar{h}_2$, and $\bar{n}_3$, on the fault surface. Then, substituting equations (9) and (12) into equation (26), we obtain

$$r = \sum_{j=1}^{2}\sum_{k=1}^{K}\sum_{l=1}^{L}\sum_{p=1}^{K}\sum_{q=1}^{L} a_{jkl} R_{jklpq} a_{jpq} \tag{28}$$

with

$$R_{jklpq} = \frac{1}{\bar{n}_3 \bar{h}_1^4}\int \frac{\partial^2 N_k(s)}{\partial s^2}\frac{\partial^2 N_p(s)}{\partial s^2} ds \int N_l(s) N_q(s)\, ds + \frac{2}{\bar{n}_3 \bar{h}_1^2 \bar{h}_2^2}\int \frac{\partial N_k(s)}{\partial s}\frac{\partial N_p(s)}{\partial s} ds \int \frac{\partial N_l(s)}{\partial s}\frac{\partial N_q(s)}{\partial s} ds + \frac{1}{\bar{n}_3 \bar{h}_2^4}\int N_k(s) N_p(s)\, ds \int \frac{\partial^2 N_l(s)}{\partial s^2}\frac{\partial^2 N_q(s)}{\partial s^2} ds \tag{29}$$

or, in vector form,

$$r = \mathbf{a}^{\mathrm{T}}\mathbf{G}\mathbf{a} \tag{30}$$

where $\mathbf{G}$ is a $M \times M$ dimensional symmetric matrix, whose IJ element is defined by

$$G_{IJ} = R_{jklpq} \tag{31}$$

with

$$I = (j-1)KL + (k-1)L + l, \qquad J = (j-1)KL + (p-1)L + q. \tag{32}$$

The integrals in equation (29) vanish when $|k - p|$ or $|l - q| \geq 4$, since $N_j(s)$ are the normalized cubic B-splines with the local support of $s_j - 2\Delta s \leq s < s_j + 2\Delta s$. Therefore $\mathbf{G}$ becomes a sparse matrix with a simple known structure.

The quantity r defined by equation (30) has a positive-definite quadratic form of $\mathbf{a}$. Therefore, using this quantity, we may represent the prior constraints on the roughness of fault slip distribution in the form of a probability density function (pdf) with a hyperparameter ρ^2 as

$$p(\mathbf{a}; \rho^2) = (2\pi\rho^2)^{-P/2} \|\mathbf{\Lambda}_P\|^{1/2} \exp\left(-\frac{1}{2\rho^2}\mathbf{a}^{\mathrm{T}}\mathbf{G}\mathbf{a}\right) \tag{33}$$

where P is the rank of the matrix $\mathbf{G}$, and $\|\mathbf{\Lambda}_P\|$ represents the absolute value of the product of non-zero eigenvalues of $\mathbf{G}$. The hyperparameter ρ^2 controls the prior distribution of $\mathbf{a}$, and hence the roughness of fault slip distribution; that is, the large value of ρ^2 permits the rough distribution of fault slip, and the small value of ρ^2 requires the smooth distribution of fault slip.

2.5 Bayesian modelling and ABIC

Now we incorporate the prior distribution $p(\mathbf{a}; \rho^2)$ in equation (33) with the data distribution $p(\mathbf{d} \mid \mathbf{a}; \sigma^2)$ in equation (25) by using Bayes' theorem, and construct a highly flexible model with the hyperparameters, σ^2 and ρ^2, called a Bayesian model:

$$p(\mathbf{a}; \sigma^2, \rho^2 \mid \mathbf{d}) = cp(\mathbf{d} \mid \mathbf{a}; \sigma^2)p(\mathbf{a}; \rho^2), \tag{34}$$

where c is a normalizing factor defined by

$$c = 1 \Big/ \int p(\mathbf{d} \mid \mathbf{a};\, \sigma^2) p(\mathbf{a};\, \rho^2)\, d\mathbf{a}. \tag{35}$$

Substituting equations (25) and (33) into equation (34), and introducing a new hyperparameter $\alpha^2 (= \sigma^2/\rho^2)$ instead of ρ^2, we obtain

$$p(\mathbf{a};\, \sigma^2,\, \alpha^2 \mid \mathbf{d}) = c(2\pi\sigma^2)^{-(N+P)/2} (\alpha^2)^{P/2} \|\mathbf{E}\|^{-1/2} \|\mathbf{A}_P\|^{1/2} \times \exp\left[-\frac{1}{2\sigma^2} s(\mathbf{a})\right], \tag{36}$$

with

$$s(\mathbf{a}) = (\mathbf{d} - \mathbf{H}\mathbf{a})^{\mathrm{T}} \mathbf{E}^{-1} (\mathbf{d} - \mathbf{H}\mathbf{a}) + \alpha^2 \mathbf{a}^{\mathrm{T}} \mathbf{G} \mathbf{a}. \tag{37}$$

Our problem is to find the values of $\mathbf{a}$, σ^2, and α^2 which maximize the posterior pdf in equation (36) for given data $\mathbf{d}$.

First we consider the case in which the hyperparameters, σ^2 and α^2, are fixed to certain values. Then the maximum of the posterior pdf is realized by minimizing $s(\mathbf{a})$ in equation (37). For any solution which minimizes $s(\mathbf{a})$, the variation of $s(\mathbf{a})$ with respect to $\mathbf{a}$ must vanish. Thus we obtain a fundamental equation to be satisfied by the solution $\mathbf{a}^*$ (Jackson & Matsu'ura 1985):

$$\mathbf{H}^{\mathrm{T}} \mathbf{E}^{-1} (\mathbf{d} - \mathbf{H}\mathbf{a}^*) - \alpha^2 \mathbf{G}\mathbf{a}^* = \mathbf{0}. \tag{38}$$

The solution of the above fundamental equation is given by

$$\mathbf{a}^* = (\mathbf{H}^{\mathrm{T}} \mathbf{E}^{-1} \mathbf{H} + \alpha^2 \mathbf{G})^{-1} \mathbf{H}^{\mathrm{T}} \mathbf{E}^{-1} \mathbf{d}. \tag{39}$$

Then, denoting

$$s(\mathbf{a}^*) = (\mathbf{d} - \mathbf{H}\mathbf{a}^*)^{\mathrm{T}} \mathbf{E}^{-1} (\mathbf{d} - \mathbf{H}\mathbf{a}^*) + \alpha^2 \mathbf{a}^{*\mathrm{T}} \mathbf{G}\mathbf{a}^* \tag{40}$$

we can rewrite $s(\mathbf{a})$ in the following form:

$$s(\mathbf{a}) = s(\mathbf{a}^*) + (\mathbf{a} - \mathbf{a}^*)^{\mathrm{T}} (\mathbf{H}^{\mathrm{T}} \mathbf{E}^{-1} \mathbf{H} + \alpha^2 \mathbf{G})(\mathbf{a} - \mathbf{a}^*). \tag{41}$$

From equations (36) and (41) we can see that the posterior distribution of $\mathbf{a}$ is Gaussian with the mean of $\mathbf{a}^*$ and the covariance of

$$\mathbf{C} = \sigma^2 (\mathbf{H}^{\mathrm{T}} \mathbf{E}^{-1} \mathbf{H} + \alpha^2 \mathbf{G})^{-1}. \tag{42}$$

Now we go back to the case in which σ^2 and α^2 are unknown parameters as well as $\mathbf{a}$. To determine the best estimates of the hyperparameters, we use a Bayesian information criterion (ABIC) proposed by Akaike (1980) on the basis of the entropy maximization principle. In the present case, where the number of adjustable hyperparameters is definite, ABIC is defined by

$$\mathrm{ABIC} = (-2) \log L(\sigma^2, \rho^2) \tag{43}$$

with

$$L(\sigma^2, \rho^2) = \int p(\mathbf{d} \mid \mathbf{a};\, \sigma^2) p(\mathbf{a};\, \rho^2)\, d\mathbf{a} \tag{44}$$

and the values of σ^2 and ρ^2 which minimize the ABIC are chosen as the best estimates of the hyperparameters. Here $L(\sigma^2, \rho^2)$ is called the marginal likelihood of σ^2 and ρ^2.

Changing the hyperparameter ρ^2 to α^2 $(= \sigma^2/\rho^2)$, and carrying out the integration in equation (44) with respect to $\mathbf{a}$, we obtain

$$L(\sigma^2, \alpha^2) = (2\pi\sigma^2)^{-(N+P-M)/2} (\alpha^2)^{P/2} \|\mathbf{E}\|^{-1/2} \|\mathbf{A}_P\|^{1/2} \times \|\mathbf{H}^{\mathrm{T}} \mathbf{E}^{-1} \mathbf{H} + \alpha^2 \mathbf{G}\|^{-1/2} \exp\left[-\frac{1}{2\sigma^2} s(\mathbf{a}^*)\right]. \tag{45}$$

The minimum of ABIC is realized by maximizing $L(\sigma^2, \alpha^2)$. Thus the necessary conditions for the minimum of ABIC are

$$\frac{\partial L(\sigma^2, \alpha^2)}{\partial \sigma^2} = 0 \tag{46}$$

and

$$\frac{\partial L(\sigma^2, \alpha^2)}{\partial \alpha^2} = 0. \tag{47}$$

Solving equation (46) for σ^2, we obtain

$$\sigma^2 = s(\mathbf{a}^*)/(N + P - M), \tag{48}$$

where $s(\mathbf{a}^*)$ is the quadratic function of $\mathbf{a}^*$ defined in equation (40). If we substitute the above expression for σ^2 into equation (47), we will obtain an equation to be solved for α^2. This equation is, however, a non-linear equation, and so we cannot solve it analytically.

We substitute equation (48) into equation (45). Then, following the definition, we may write the ABIC in the form of

$$\mathrm{ABIC}(\alpha^2) = (N + P - M) \log s(\boldsymbol{a}^*) - P \log \alpha^2 + \log \|\mathbf{H}^{\mathrm{T}} \mathbf{E}^{-1} \mathbf{H} + \alpha^2 \mathbf{G}\| + C \tag{49}$$

where C is a constant term independent of α^2. The search for the value of α^2 which minimizes the ABIC can be carried out numerically. Once the value of α^2 minimizing the ABIC has been found, denoting it by $\hat{\alpha}^2$, we can obtain the best estimate of $\mathbf{a}$ from equation (39) as

$$\hat{\mathbf{a}} = (\mathbf{H}^{\mathrm{T}} \mathbf{E}^{-1} \mathbf{H} + \hat{\alpha}^2 \mathbf{G})^{-1} \mathbf{H}^{\mathrm{T}} \mathbf{E}^{-1} \mathbf{d} \tag{50}$$

and the best estimate of σ^2 from equation (48) as

$$\hat{\sigma}^2 = s(\hat{\mathbf{a}})/(N + P - M) \tag{51}$$

with

$$s(\hat{\mathbf{a}}) = (\mathbf{d} - \mathbf{H}\hat{\mathbf{a}})^{\mathrm{T}} \mathbf{E}^{-1} (\mathbf{d} - \mathbf{H}\hat{\mathbf{a}}) + \hat{\alpha}^2 \hat{\mathbf{a}}^{\mathrm{T}} \mathbf{G}\hat{\mathbf{a}}. \tag{52}$$

The covariance for the estimation errors of $\hat{\mathbf{a}}$ is calculated from equation (42) as

$$\mathbf{C} = \hat{\sigma}^2 (\mathbf{H}^{\mathrm{T}} \mathbf{E}^{-1} \mathbf{H} + \hat{\alpha}^2 \mathbf{G})^{-1}. \tag{53}$$

3 A NUMERICAL EXPERIMENT

In the preceding section we developed a new method of geodetic data inversion by using Akaike's Bayesian Information Criterion (ABIC). Now we examine the validity of this inversion method through a numerical experiment. The numerical experiment is done in the following way. (1) Give a true slip distribution on a fault plane embedded in an elastic half-space. (2) Compute surface displacements at observation points. (3) Make a set of synthesized data by adding random noise to the theoretical displacements. (4) Invert the synthesized data and reconstruct the slip distribution. The validity of our inversion method will be

checked by comparing the inverted slip distribution with the true slip distribution.

3.1 A true slip distribution and synthesized data

We consider a right-lateral, reverse faulting on a low-angle, rectangular plane embedded in an elastic half-space as shown in Fig. 3(a). On this fault plane we continuously distribute slip vectors with a uniform direction (slip-angle = 120°) but different magnitudes. The distribution of slip magnitudes is shown in Fig. 3(b). The slip magnitude distribution has a broad main-peak of 7.4 m and a subpeak of 3.5 m. For this slip distribution, using the theoretical relation (8), we compute horizontal surface displacements at 50 observation points and vertical surface displacements at 105 observation points. Then, adding random noise with zero mean and 3.4×10^{-3} m standard deviation to these theoretical surface displacements, we make a set of synthesized data. The synthesized surface displacement data are shown in Figs 4(a) (horizontal component) and (b) (vertical component) with the locations of observation points. Here it should be noted that the synthesized data are very accurate and the data coverage is almost complete.

3.2 ABIC and inverted slip distributions

We divide the rectangular model fault region ABCD in Fig. 3 into 18×9 subsections and distribute 15×6 bicubic B-splines so that they cover homogeneously the whole model fault region. The distribution of each slip component (Δu_1 or Δu_2) on the rectangular fault plane is represented by the superposition of the 15×6 bicubic B-splines with various amplitudes. Therefore the number of model parameters sums to 180. Following the procedure described in the preceding section, we construct a Bayesian model with the hyperparameters, σ^2 and α^2 $(=\sigma^2/\rho^2)$, which controls the structure of the parametric model. Then our problem is to determine the optimal values of the 180 model parameters and the two hyperparameters from the 205 synthesized surface displacement data.

First we search numerically for the value of α^2 which minimizes the ABIC defined in equation (49). From Fig. 5, where the ABIC is plotted as a function of α^2, we can find that the ABIC takes the minimum at $\alpha^2 = 2.3 \times 10^{-6}$. Once the optimal value of α^2 is determined, the best estimates of the model parameters **a** and the hyperparameter σ^2 are directly computed from equations (50) and (51). In Fig. 6(a)

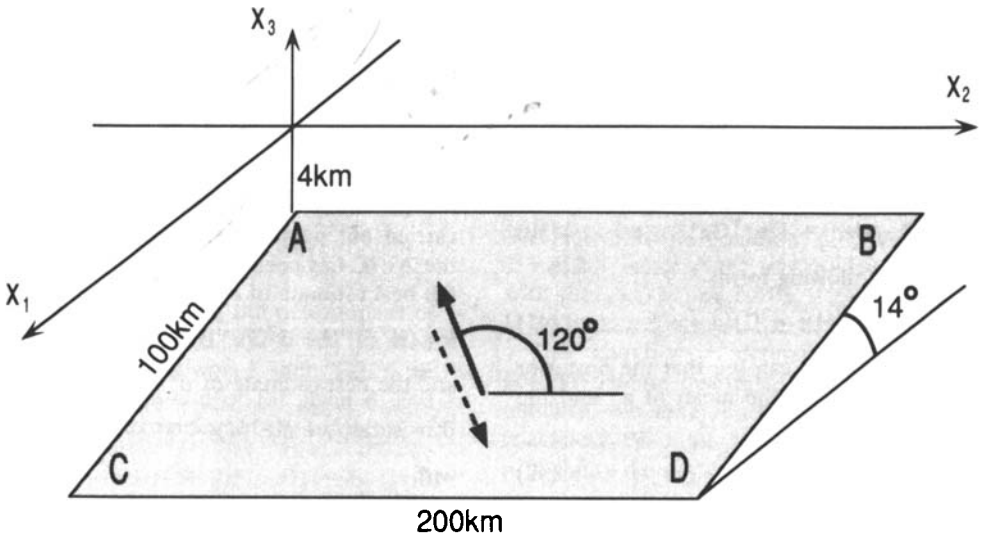

(a)

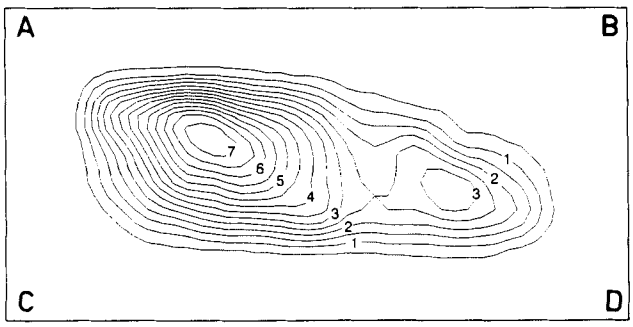

(b)

Figure 3. The true fault model used for the numerical experiment. (a) Fault geometry and slip direction. (b) Distribution of slip magnitude. The contour intervals are 0.5 m. The slip magnitude tends to zero at the fault margins.

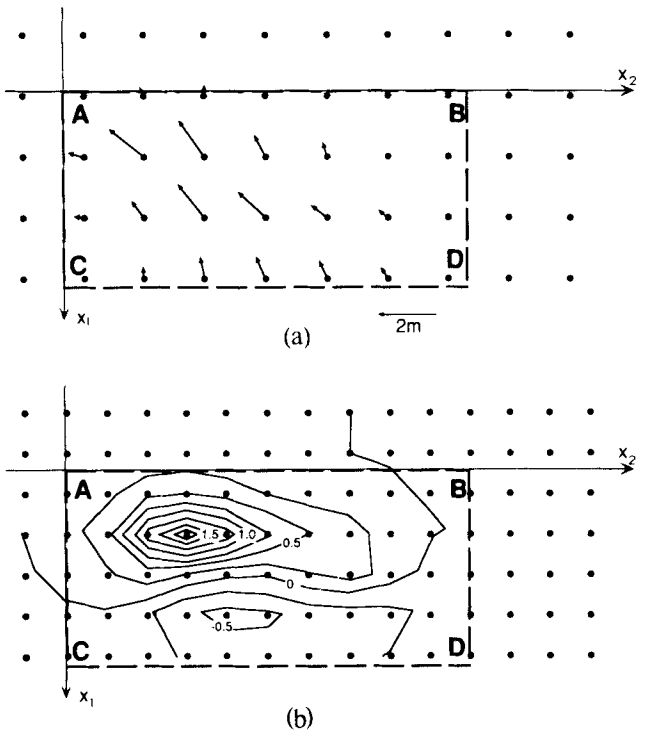

Figure 4. The surface displacement data used for the numerical experiment. (a) Horizontal displacements. (b) Vertical displacements. The rectangle ABCD indicates the projection of the model fault region on the surface. The solid circles indicate observation points.

we show the spatial distribution of slip vectors on the rectangular fault plane, reconstructed by substituting the best estimates of **a** into equation (9). The corresponding slip magnitude distribution is given in Fig. 6(b). Comparing Fig. 6 with Fig. 3, we can see that the true slip distribution is almost completely reconstructed in the case of ABIC minimum.

To demonstrate the validity of ABIC we show the inverted slip distributions for the inappropriate choice of the value of α^2. Fig. 7 is the case in which the value of α^2 is

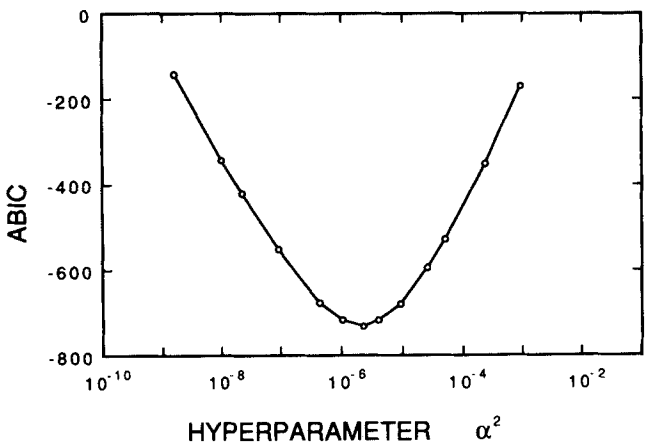

Figure 5. The values of ABIC plotted as a function of α^2. The ABIC takes the minimum at $\alpha^2 = 2.3 \times 10^{-6}$.

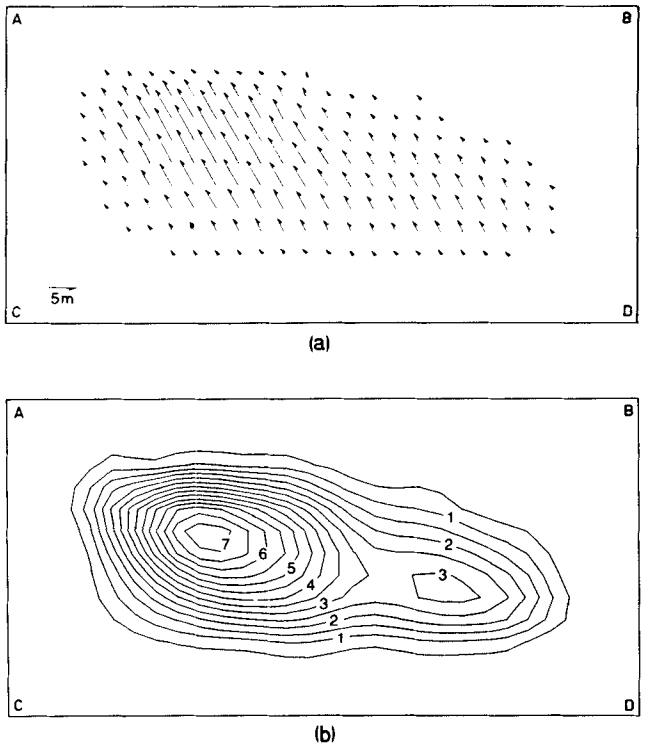

Figure 6. The optimal fault slip distribution inverted from the synthesized surface displacement data. (a) Distribution of slip vectors. (b) Distribution of slip magnitude. The rectangle ABCD indicates the model fault region. The contour intervals are the same as those in Fig. 3.

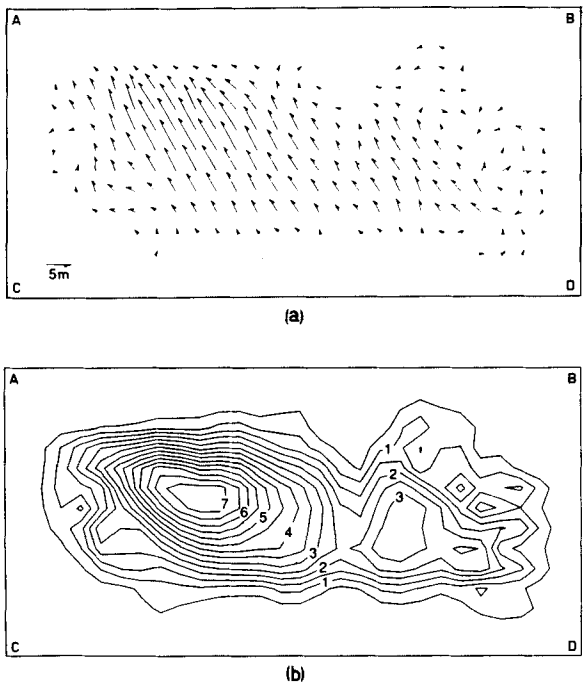

Figure 7. The inverted fault slip distribution when the value of α^2 is too small. (a) Distribution of slip vectors. (b) Distribution of slip magnitude.

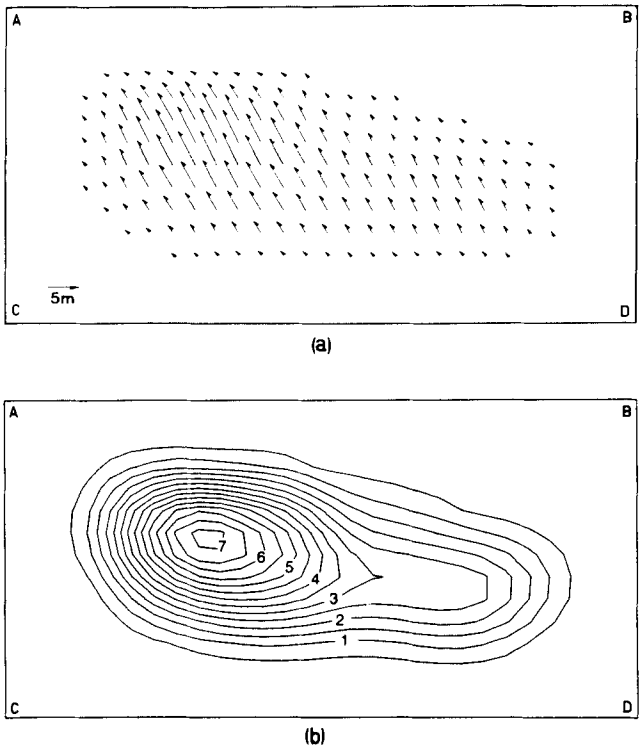

Figure 8. The inverted fault slip distribution when the value of α^2 is too large. (a) Distribution of slip vectors. (b) Distribution of slip magnitude.

much smaller than its optimal value. The smaller the value of α^2, the weaker the prior constraint on the roughness of slip distribution. Thus, as we can expect, the inverted slip distribution becomes very irregular both in slip direction and slip magnitude. On the other hand, when the value of α^2 is much greater than its optimal value, the inverted slip distribution becomes very smooth as shown in Fig. 8. In this case the subpeak of 3.5 m existing in the true slip distribution disappears, because the prior constraint is too strong. It should be noted that these slip distributions are also the best solutions in the sense of the maximum likelihood. ABIC enable us to select only one solution from among them as the optimal slip distribution.

The closeness of the inverted slip distribution to the true distribution is not necessarily a good indicator to check whether the present inversion method is consistent or not, because it depends on the accuracy and sufficiency of data. For example, when the added random noise is 10 times as large as that in the present case, we obtain a very smooth slip distribution just like that in Fig. 8 as the optimal solution. One of the ways to check the consistency of the method is to compare the estimate of σ^2 obtained from equation (51) with its true value ($1 \times 10^{-5}\,\mathrm{m}^2$). In Table 1 we show the estimates of σ^2 for the three representative cases corresponding to Figs 6, 7, and 8. In Case 1 (the case of ABIC minimum) the value of σ^2 is correctly estimated. This warrants that our choice of α^2 based on ABIC is appropriate. In Case 2 the value of σ^2 is underestimated. The irregular slip distribution in Fig. 7 is ascribed to random noise in the data. In Case 3 the value of σ^2 is fairly overestimated. The reason why the slip distribution in Fig. 8 is too smooth is because a part of the useful information in data has been discarded as noise.

4 APPLICATION TO THE 1946 NANKAIDO EARTHQUAKE

As an example we consider the case of the 1946 Nankaido earthquake. For this earthquake coseismic surface displacements have been revealed in detail from the comparison of the pre- and post-seismic geodetic measurements. We apply the new inversion method developed in Section 2 to the coseismic displacement data and reconstruct the fault slip distribution of this earthquake. Through this inversion analysis we demonstrate the applicability of the new inversion method to actual cases.

4.1 The 1946 Nankaido earthquake

In southwest Japan the Philippine Sea plate is descending beneath the Eurasian plate at the Nankai trough with the convergence rate of $4\,\mathrm{cm\,yr}^{-1}$. The 1946 Nankaido earthquake ($M_s = 8.2$) is a great thrust-type earthquake that occurred along this plate boundary. In Fig. 9 we show the location of the epicentre and the tsunami source area of the Nankaido earthquake, determined by Kanamori (1972) and Hatori (1974) respectively, with those of the 1944 Tonankai earthquake ($M_s = 8.0$).

The faulting mechanism of the 1946 Nankaido earthquake has been studied by many investigators: Kanamori (1972) on the basis of seismological data, Fitch & Scholz (1971) and Ando (1975) on the basis of geodetic data, and Aida (1981) and Ando (1982) on the basis of tsunami data. The fault models proposed by these authors are summarized in Table 2. Because of the different sources of information and the different criteria for model selection, the derived fault parameters should not be directly compared. Nevertheless, considering the very low reliability in the estimation of source dimensions from seismological data, we can find some common features to these models: (1) the faulting region extends from Shikoku Island to Kii Peninsula along the Nankai trough; (2) the direction of fault slip is roughly in accord with that of plate convergence (N50°W) at the Nankai trough; and (3) the amount of slip in the western half of the faulting region is significantly larger than that in the eastern half.

Table 1. The estimates of σ^2 for three representative cases.

CASE	α^2	$\sigma^2(\mathrm{m}^2)$	*ABIC*(C=0)	PRIOR CONSTRAINT
1	2.3×10^{-6}	1×10^{-5}	-731	appropriate
2	2.3×10^{-8}	3×10^{-6}	-421	weak
3	2.3×10^{-4}	1×10^{-3}	-351	strong

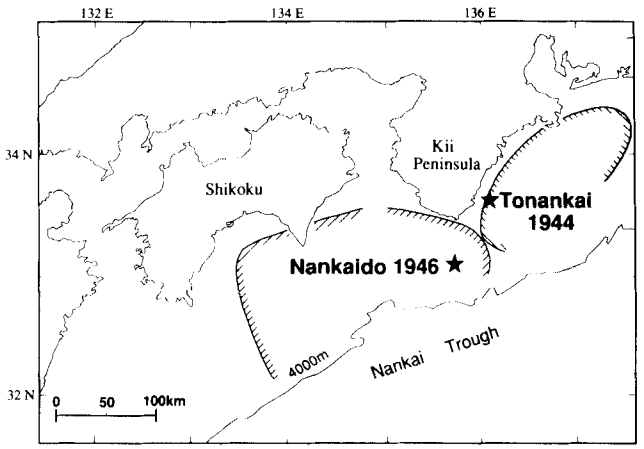

Figure 9. Location map showing the epicentres (stars) and the tsunami source areas (hatched areas) of the 1944 Tonankai and the 1946 Nankaido earthquakes.

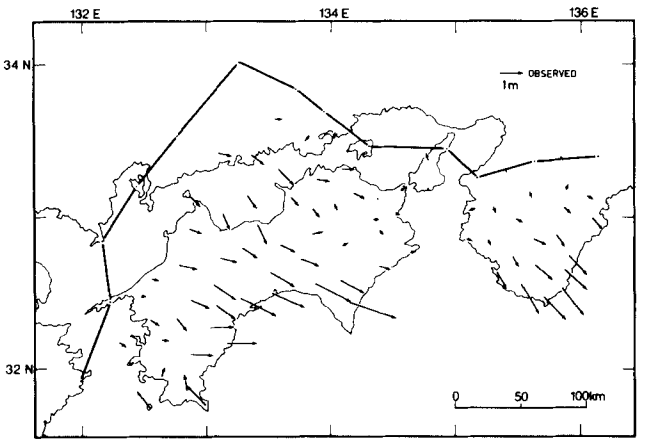

Figure 10. Coseismic horizontal displacements at triangulation points, derived from the comparison of the pre-seismic measurements (1860–1899) and the post-seismic measurements (1947–1948). The triangulation points connected by the thick solid lines indicate the reference points used for the comparison of the pre- and post-seismic measurements.

4.2 Surface displacement data

The surface displacements associated with the 1946 Nankaido earthquake have been revealed in detail from the comparison of the pre- and post-seismic geodetic measurements by the Geographical Survey Institute of Japan (1952, 1955). In the present inversion analysis we use the horizontal displacement data at 92 triangulation points shown in Fig. 10 and the vertical displacement data at 181 bench marks shown in Fig. 11. Within the period between the pre- and post-seismic measurements, another great earthquake, the 1944 Tonankai earthquake, had occurred in the eastern part of Kii Peninsula. Therefore the data used here contain the surface displacements caused by this earthquake as a part. This must be called to mind when we interpret the inverted result.

The surface displacement data derived from the comparison of the geodetic measurements contain the systematic errors resulting from the movements of reference points. If the displacements of the reference points are known, we can correct the data by subtracting the apparent displacements induced by the rotation and expansion (or contraction) of base lines. In the present case, however, the displacements of the reference points are unknown, and so we must treat them as unknown parameters in the inversion analysis. The mathematical treatment of this problem is given in Matsu'ura *et al.* (1980).

We suppose that the data errors remaining after the subtraction of the systematic errors are Gaussian with zero mean and covariance $\sigma^2\mathbf{E}$. The data errors consist of measurement errors and modelling errors. The measurement errors in triangulation are generally much greater than those in levelling. The modelling errors will be roughly in proportion to the absolute values of observed displace-

Table 2. The fault models of the 1946 Nankaido earthquake derived from various kinds of data. The slip-angle is measured counterclockwise from the horizon on each fault plane. The fault patches are numbered from the west to the east.

		STRIKE	DIP-ANGLE	SLIP-ANGLE	LENGTH(km)	WIDTH(km)	SLIP(m)	DATA
Fitch &	F1	N70°E	30°NW	90°	40	95	18.0	geodetic
Scholz	F2	N70°E	30°NW	90°	30	140	18.0	data
(1971)	F3	N70°E	30°NW	90°	20	100	15.0	
	F4	N70°E	30°NW	90°	40	70	10.0	
	F5	N70°E	40°NW	90°	95	50	8.0	
Kanamori		N40°E	10°NW	90°	120	80	3.1	seismic
(1972)								data
Ando	F1	N70°E	20°NW	117°	150	120	6.0	geodetic
(1975)	F2	N70°E	25°NW	117°	150	70	4.0	data
Aida	F1	N70°E	20°NW	104°	120	120	5.0	tsunami
(1981)	F2	N70°E	10°NW	127°	150	70	4.0	data
Ando	F1	N70°E	20°NW	117°	150	70	6.0	geodetic
(1982)	F2	N70°E	25°NW	117°	150	70	3.0	data

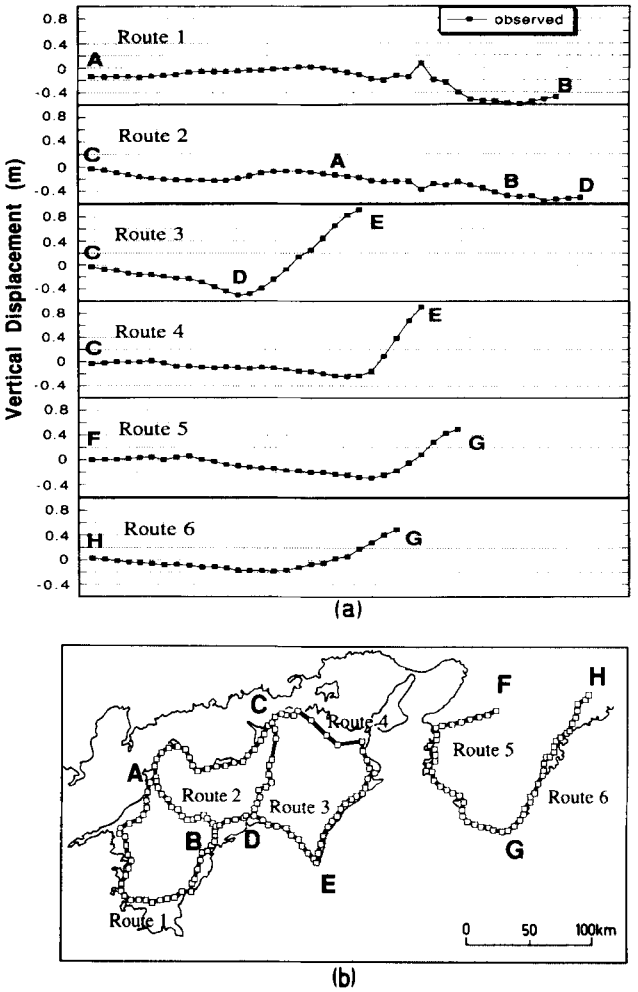

Figure 11. Coseismic vertical displacements (a) along the levelling routes (b), derived from the comparison of the pre-seismic measurements (1910–1940) and the post-seismic measurements (1947–1948). The bench mark F was taken as the reference point for the comparison of the pre- and post-seismic measurements.

ments. From these considerations we take the matrix elements of **E** as

$$E_{ij} = (\beta^2 + \gamma^2 |d_i/d_o|^2)\,\delta_{ij} \tag{54}$$

with $\beta = 1$, $\gamma = 1$, and $d_0 = 1$ m for vertical displacements, and $\beta = 2$, $\gamma = 2$, and $d_0 = 1$ m for horizontal displacements.

4.3 The fault model used for inversion

It will be a reasonable assumption that the main slip of the 1946 Nankaido earthquake occurred along the boundary between the Philippine Sea plate and the Eurasian plate. The configuration of the upper boundary of the descending Philippine Sea plate in southwest Japan can be determined from the distribution of microearthquakes (Mizoue *et al.* 1983; Takagi & Matsuzawa 1987). Fig. 12 shows the isodepth contours of the upper boundary of the Philippine Sea plate, determined from the distribution of microearthquakes. The dip-angle of the plate boundary is very low (about 10°) beneath Shikoku Island and relatively high (about 15°) beneath Kii Peninsula. The abrupt change

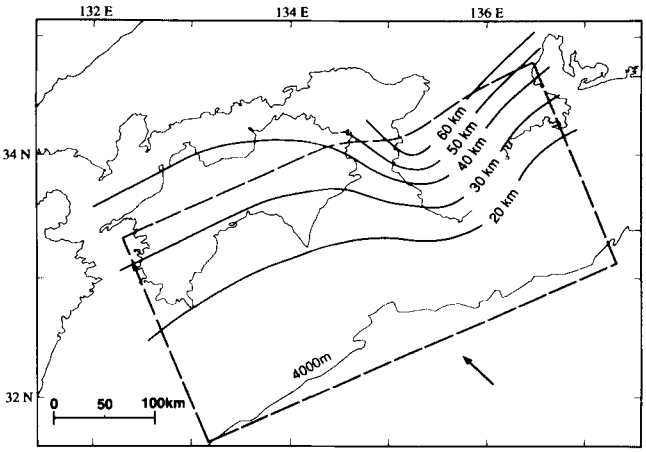

Figure 12. Isodepth contours of the upper boundary of the Philippine Sea plate, determined from the distribution of microearthquakes. The area enclosed by the broken line indicates the surface projection of the model fault region taken on the curved plate boundary.

in the dip-angle of the plate boundary occurs along Kii Strait.

On this curved plate boundary we take a model fault region as shown in Fig. 12. We divide this model fault region into 24×12 subsections and distribute 21×9 bicubic B-splines so that they cover homogeneously the whole model fault region. The distribution of each slip component (Δu_1 or Δu_2) on the curved fault surface is represented by the superposition of the 21×9 bicubic B-splines with various amplitudes. Therefore the number of model parameters sums up to 405, including 27 unknown parameters for the displacements of reference points in geodetic measurements. Following the procedure described in Section 2, we construct a Bayesian model with the hyperparameters, σ^2 and α^2 $(=\sigma^2/\rho^2)$. Then our problem is to determine the optimal values of these two hyperparameters and the 405 model parameters from the 365 observed surface displacement data.

The occurrence of great earthquakes at plate boundaries is now understood as the process of releasing the tectonic stress caused by relative plate motion. This implies that the slip vectors of interplate earthquakes must be in the direction parallel to the relative plate motion on the whole. We may use such a knowledge of the slip directions as prior information. At the Nankai trough, according to Seno (1977), the direction of plate convergence is about N50°W. Therefore, in the present inversion analysis, we constrain the direction of slip vectors within the range of N50°W ± 45°; that is,

$$(\tan 65°)\Delta u_1 \le \Delta u_2 \le -(\tan 25°)\Delta u_1 \tag{55}$$

where Δu_1 and Δu_2 indicate respectively the slip components perpendicular and parallel to the strike (N110°W) of the Nankai trough. Substituting the expressions of Δu_1 and Δu_2 in equation (9) into equation (55), we obtain linear inequality constraints on the model parameters **a**.

To find the maximum likelihood estimates of **a** under the linear inequality constraints, we can use the algorithm of

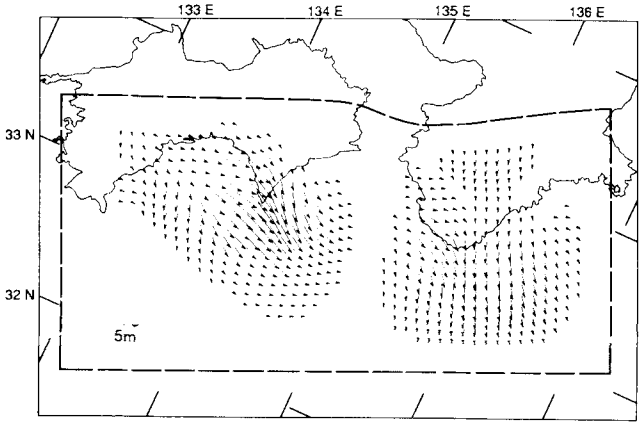

Figure 13. The distribution of slip vectors inverted from the observed surface displacement data. The area enclosed by the broken lines indicates the model fault region.

non-negative least-squares (NNLS) by Lawson & Hanson (1974). Once the maximum likelihood estimates of **a** have been obtained, the following procedure to find the minimum of ABIC is essentially the same as that described in Section 2.

4.4 The inverted slip distribution

By using the fault model described in Section 4.3, we inverted the surface displacement data given in Section 4.2 under the linear inequality constraints (55). The result is shown in Fig. 13. The inverted slip distribution has the two high-slip areas separated by the low-slip zone extending along Kii Strait. The tsunami source area of the 1946 Nankaido earthquake, which is shown in Fig. 9, covers the whole of the western high-slip area and the western half of the eastern high-slip area. The eastern half of the eastern high-slip area corresponds to the source area of the 1944 Tonankai earthquake. The direction of dominant slip motion is in accord with that of plate convergence on the whole, but it deviates eastward about 20° from the direction of plate convergence (S50°E) in the western high-slip area and westward about 20° in the eastern high-slip area.

Fig. 14 is the contour map showing the distribution of

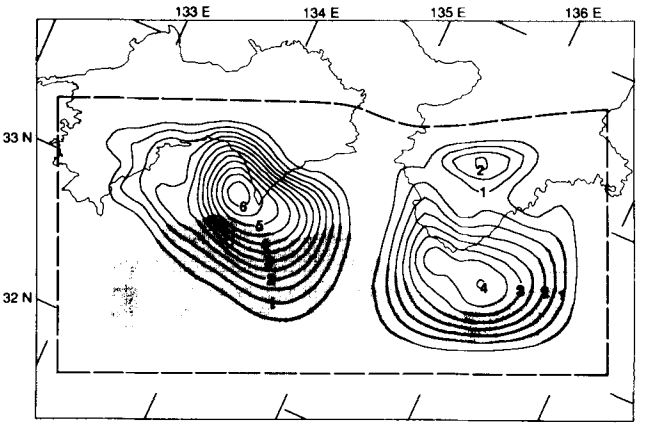

Figure 14. Contour map showing the distribution of slip magnitude with estimation errors. The contour intervals are 0.5 m. The area with large estimation errors (≥1.5 m) is shaded.

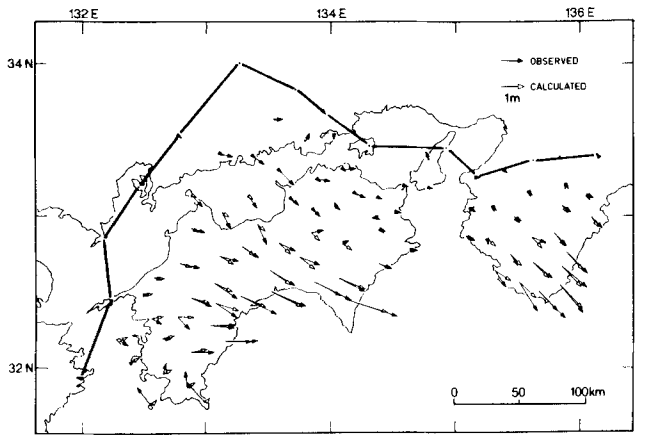

Figure 15. Comparison of the horizontal displacements (white-headed arrows) calculated from the inverted fault slip model with the observed data (black-headed arrows). The triangulation points connected by the thick solid lines indicate the reference points in triangulation.

slip magnitude with the estimation errors calculated from equation (53). It should be noted that the estimation errors shown here are those for the optimal solution obtained without the constraints on the direction of slip vectors. The amount of fault slip reaches 6.4 m at the centre of the western high-slip area. The maximum fault slip in the eastern high-slip area is 4.0 m. The large estimation errors in the region off land are clearly due to the lack of observed data. From this contour map we can see that the dominant fault slip occurs in the region shallower than 30 km in depth.

In Fig. 15 we compare the horizontal displacements calculated from the inverted fault slip model with the observed data. The calculated horizontal displacements contain the effects of the displacements of reference points. The

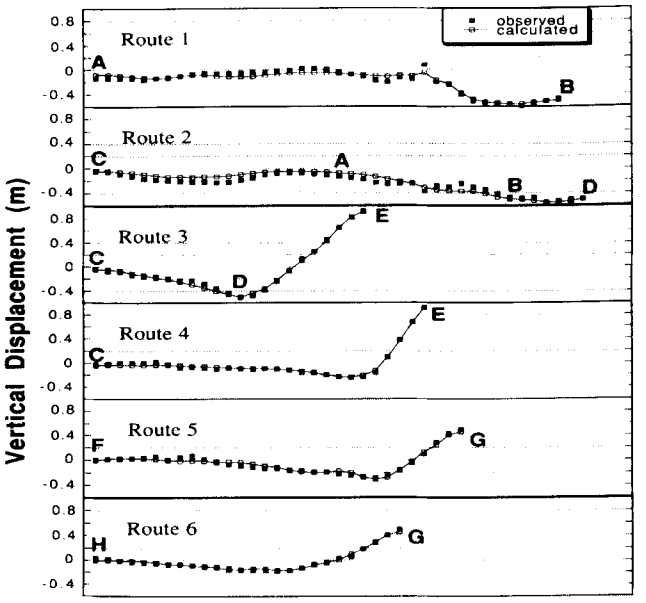

Figure 16. Comparison of the vertical displacements (open squares) calculated from the inverted fault slip model with the observed data (solid squares). The numbers of levelling routes correspond to those in Fig. 11.

observed horizontal displacements are well explained by the inverted fault model except for a few data in the southwestern part of Skikoku Island. In Fig. 16 the calculated vertical displacements along the levelling routes are compared with the observed data. The numbers of the levelling routes correspond to those in Fig. 11. The observed vertical displacements are almost completely explained by the inverted fault model. The value of σ^2 estimated from equation (51) is $5^2 \times 10^{-4}\,\mathrm{m}^2$. This means that the data errors, including measurement errors and modelling errors, are about 5–7 cm for the vertical displacements and 10–20 cm for the horizontal displacements.

5 DISCUSSION AND CONCLUSIONS

Coseismic surface displacement data contain useful information about the spatial distribution of fault slip at the time of an earthquake. To extract the unbiased information through the inversion analysis of the data, we need an appropriate parametric model that relates the surface displacements with the fault slip distribution. If the appropriate parametric model has been given, we are able to determine the optimal values of the model parameters by using the maximum likelihood criterion. Then how can we choose the appropriate parametric model? As we demonstrated in the present paper, Akaike's Bayesian Information Criterion (ABIC) gives us an answer to this question.

We developed a new inversion method to reconstruct the spatial distribution of fault slip from the surface displacement data, using ABIC. In this method, first, the fault slip distribution is represented by the superposition of bicubic B-splines with various amplitudes. Then, incorporating prior information about the smoothness of fault slip distribution with the information coming from the observed surface displacement data, we construct a parametric model with a highly flexible structure controlled by hyperparameters. This model, called a Bayesian model, consists of a family of parametric models. From among the family of parametric models we can select the most appropriate parametric model by using ABIC. Once the appropriate parametric model has been selected, the following procedure to find the best estimates of the model parameters is essentially the same as that in the maximum likelihood method. We demonstrated the validity of the new inversion method through the numerical experiment using theoretical surface displacement data with random errors.

By using the new inversion method we analysed the surface displacement data associated with the 1944 Tonankai and the 1946 Nankaido earthquakes. The inverted fault slip distribution is characterized by the two high-slip areas separated by a low-slip zone extending along Kii Strait. The source area of the 1946 Nankaido earthquake, estimated from tsunami data, covers the whole of the western high-slip area and the western half of the eastern high-slip area. The hypocentre of this earthquake is located at the centre of the eastern high-slip area. The eastern half of the eastern high-slip area corresponds to the source area of the 1944 Tonankai earthquake. The direction of dominant fault slip motion deviates eastward about 20° from the direction of plate convergence (S50°E) in the western high-slip area and westward about 20° in the eastern high-slip area. The maximum fault slip is 6.4 m in the western high-slip area and 4.0 m in the eastern high-slip area. These features of the inverted fault slip distribution seem to be closely related with the difference in rupture process between the eastern and western areas, pointed out by the former investigators. Another interesting feature revealed from the present inversion analysis is that the dominant fault slip occurs in the region shallower than 30 km in depth. The depth of 30 km may indicate the lower bound of the seismogenic zone in southwest Japan.

REFERENCES

Aida, I., 1981. Numerical simulations of the off-Nankaido tsunami, *Bull Earthq. Res. Inst. Tokyo Univ.*, **56,** 713–730 (in Japanese).

Akaike, H., 1977. On entropy maximization principle, in *Application of Statistics,* pp. 27–41, ed. Krishnaiah, P. R., North-Holland, Amsterdam.

Akaike, H., 1980. Likelihood and the Bayes procedure, in *Bayesian Statistics,* pp. 143–166, eds Bernardo, J. M., DeGroot, M. H., Lindley, D. V. & Smith, A. F. M., University Press, Valencia, Spain.

Ando, M., 1975. Source mechansims and tectonic significance of historical earthquakes along the Nankai trough, Japan, *Tectonophysics,* **27,** 119–140.

Ando, M., 1982. A fault model of the 1946 Nankaido earthquake derived from tsunami data, *Phys. Earth planet. Inter.*, **28,** 320–336.

Backus, G. & Gilbert, F., 1970. Uniqueness in the inversion of inaccurate gross Earth data, *Phil. Trans. R. Soc. Lond.*, A, **266,** 123–192.

Backus, G. & Mulcahy, M., 1976a. Moment tensors and other phenomenological descriptions of seismic sources—I. Continuous displacements, *Geophys. J. R. astr. Soc.*, **46,** 341–361.

Backus, G. & Mulcahy, M., 1976b. Moment tensors and other phenomenological descriptions of seismic sources—II. Discontinuous displacements, *Geophys. J. R. astr. Soc.*, **47,** 301–329.

Barrientos, S. E., 1988. Slip distribution of the 1985 Central Chile earthquake, *Tectonophysics,* **145,** 225–241.

Burridge, R. & Knopoff, L., 1964. Body force equivalents for seismic dislocations, *Bull. seism. Soc. Am.*, **54,** 1875–1888.

Cox, M. G., 1972. The numerical evaluation of B-splines, *J. Inst. Math. Appl.*, **10,** 134–149.

de Boor, C., 1972. On calculating with B-splines, *J. Approx. Theory,* **6,** 50–62.

Fisher, R. A., 1922. On the mathematical formulations of theoretical statistics, *Phil. Trans. R. Soc. Lond.*, A, **222,** 309–368.

Fitch, T. J. & Scholz, C. H., 1971. Mechanism of underthrusting in southwest Japan: A model of convergent plate interactions, *J. geophys. Res.*, **76,** 7260–7292.

Geographical Survey Institute of Japan, 1952. Resurvey of the southwestern part of Japan after the great Nankaido earthquake of 1946 (Report No. 1: Results on the first-order triangulation), *Bull. Geog. Surv. Inst.*, **3,** 31–118.

Geographical Survey Institute of Japan, 1955. *Collection of the Results of Precise Leveling along Primary Bench Marks*, vol. 1, Geograph. Surv. Inst., Ministry of Construction, Chiba, Japan (in Japanese).

Hatori, T., 1974. Sources of large tsunamis in southwest Japan, *J. seism. Soc. Japan, Ser.* 2, **27,** 10–24 (in Japanese with English abstract).

Jackson, D. D., 1979. The use of a priori data to resolve nonuniqueness in linear inversion, *Geophys. J. R. astr. Soc.*, **57,** 137–157.

Jackson, D. D. & Matsu'ura, M., 1985. A Bayesian approach to nonlinear inversion, *J. geophys. Res.*, **90,** 581–591.

Kanamori, H., 1972. Tectonic implication of the 1944 Tonankai and the 1946 Nankaido earthquakes, *Phys. Earth planet. Inter.*, **4**, 129–139.

Lawson, C. L. & Hanson, R. J., 1974. *Solving Least Squares Problems*, Prentice-Hall, Englewood Cliffs, NJ.

Maruyama, T., 1963. On the force equivalents of dynamic elastic dislocations with reference to the earthquake mechanism, *Bull. Earthq. Res. Inst. Tokyo Univ.*, **41**, 467–486.

Maruyama, T., 1964. Statical elastic dislocations in an infinite and semi-infinite medium, *Bull. Earthq. Res. Inst. Tokyo Univ.*, **42**, 289–368.

Matsu'ura, M., 1977a. Inversion of geodetic data. Part I: Mathematical formulation, *J. Phys. Earth*, **25**, 69–90.

Matsu'ura, M., 1977b. Inversion of geodetic data. Part II: Optimal model of conjugate fault system for the 1927 Tango earthquake, *J. Phys. Earth*, **25**, 233–255.

Matsu'ura, M. & Hasegawa, Y., 1987. A maximum likelihood approach to nonlinear inversion under constraint, *Phys. Earth planet. Inter.*, **47**, 179–187.

Matsu'ura, M., Iwasaki, T., Suzuki, Y. & Sato, R., 1980. Statical and dynamical study on faulting mechanism of the 1923 Kanto earthquake, *J. Phys. Earth*, **28**, 119–143.

Miyashita, Y. & Matsu'ura, M., 1978. Inversion analysis of static displacement data associated with the Alaska earthquake of 1964, *J. Phys. Earth*, **26**, 333–349.

Mizoue, M., Nakamura, M., Seto, N., Ishiketa, Y. & Yokota, T., 1983. Three-layered distribution of microearthquakes in relation to focal mechanism variation in the Kii peninsula, southwestern Honshu, Japan, *Bull. Earthq. Res. Inst. Tokyo Univ.*, **58**, 287–310.

Seno, T., 1977. The instantaneous rotation vector of the Philippine Sea plate relative to the Eurasian plate, *Tectonophysics*, **42**, 209–226.

Takagi, A. & Matsuzawa, T., 1987. Microseismic activity in Japan (July, 1983–June, 1984), in *Proceedings of Earthquake Prediction Research Symposium (1987)*, pp. 17–30, National Committee for Seismology, Science Council of Japan & Seismological Society of Japan, Tokyo (in Japanese).

Tarantola, A. & Valette, B., 1982a. Inverse problems = Quest for information, *J. geophys. Res.*, **50**, 159–170.

Tarantola, A. & Valette, B., 1982b. Generalized nonlinear inverse problems solved using the least squares criterion, *Rev. Geophys. Space Phys.*, **20**, 219–232.

Ward, S. N. & Barrientos, S. E., 1986. An inversion for slip distribution and fault shape from geodetic observations of the 1983 Borah Peak, Idaho, earthquake, *J. geophys. Res.*, **91**, 4909–4919.

APPENDIX A

We consider an isotropic, homogeneous, elastic half-space ($x_3 \leq 0$) with Lamé's constants λ and μ. The ith component $u_i(\mathbf{x})$ of surface displacement due to the moment tensor density $m_{pq}(\xi)$ distributed on a fault surface S can be expressed as

$$u_i(\mathbf{x}) = \sum_{p=1}^{3}\sum_{q=1}^{3}\int_S G_{ip,q}(\mathbf{x}, \xi) m_{pq}(\xi)\, dS(\xi) \quad (i = 1, 2, 3) \tag{A1}$$

where $G_{ip,q}$ indicates the derivative of Green's tensor G_{ip} with respect to ξ_q. Because of the symmetry of m_{pq}, $G_{ip,q}$ and $G_{iq,p}$ appear always in pairs. Concrete expressions for the spatial derivatives of Green's tensor are given as follows:

$$G_{11,1} = (1/4\pi\mu)(X/R^3)[F_1 X^2/R^2 + 3\gamma/(z+1)^2 - 1], \tag{A2}$$

$$G_{12,2} = (1/4\pi\mu)(X/R^3)[F_1 Y^2/R^2 + \gamma/(z+1)^2 - 1], \tag{A3}$$

$$G_{13,3} = (1/4\pi\mu)(X/R^3)[3z^2 + \gamma - 1], \tag{A4}$$

$$G_{11,2} + G_{12,1} = (1/2\pi\mu)(Y/R^3)[F_1 X^2/R^2 + \gamma/(z+1)^2], \tag{A5}$$

$$G_{11,3} + G_{13,1} = (3/2\pi\mu)(X^2/R^4)z, \tag{A6}$$

$$G_{12,3} + G_{13,2} = (3/2\pi\mu)(XY/R^4)z, \tag{A7}$$

$$G_{21,1} = (1/4\pi\mu)(Y/R^3)[F_1 X^2/R^2 + \gamma/(z+1)^2 - 1], \tag{A8}$$

$$G_{22,2} = (1/4\pi\mu)(Y/R^3)[F_1 Y^2/R^2 + 3\gamma/(z+1)^2 - 1], \tag{A9}$$

$$G_{23,3} = (1/4\pi\mu)(Y/R^3)[3z^2 + \gamma - 1], \tag{A10}$$

$$G_{21,2} + G_{22,1} = (1/2\pi\mu)(X/R^3)[F_1 Y^2/R^2 + \gamma/(z+1)^2], \tag{A11}$$

$$G_{21,3} + G_{23,1} = (3/2\pi\mu)(XY/R^4)z, \tag{A12}$$

$$G_{22,3} + G_{23,2} = (3/2\pi\mu)(Y^2/R^4)z, \tag{A13}$$

$$G_{31,1} = (1/4\pi\mu)(1/R^2)[F_2 X^2/R^2 - z + \gamma/(z+1)], \tag{A14}$$

$$G_{32,2} = (1/4\pi\mu)(1/R^2)[F_2 Y^2/R^2 - z + \gamma/(z+1)], \tag{A15}$$

$$G_{33,3} = (1/4\pi\mu)(1/R^2)[3z^3 + (\gamma - 1)z], \tag{A16}$$

$$G_{31,2} + G_{32,1} = (1/2\pi\mu)(XY/R^4)F_2, \tag{A17}$$

$$G_{31,3} + G_{33,1} = (3/2\pi\mu)(X/R^3)z^2, \tag{A18}$$

$$G_{32,3} + G_{33,2} = (3/2\pi\mu)(Y/R^3)z^2, \tag{A19}$$

where

$$X = x_1 - \xi_1, \quad Y = x_2 - \xi_2, \quad Z = -\xi_3, \quad R = \sqrt{X^2 + Y^2 + Z^2} \tag{A20}$$

and

$$z = Z/R, \quad F_1 = 3 - \gamma(z+3)/(z+1)^3, \quad F_2 = 3z - \gamma(z+2)/(z+1)^2, \tag{A21}$$

with

$$\gamma = \mu/(\lambda + \mu). \tag{A22}$$

APPENDIX B

Concrete expressions for cubic B-splines $M_{4,j}(s)$ with equally spaced local support $(s_j - 4\Delta s \leq s < s_j)$ are given by

$$24\Delta s^4 M_{4,j}(s) = \begin{cases} (s - s_j + 4\Delta s)^3, & s_j - 4\Delta s \leq s < s_j - 3\Delta s, \\ (s - s_j + 4\Delta s)^2(s_j - 2\Delta s - s) + (s - s_j + 4\Delta s)(s - s_j + 3\Delta s)(s_j - \Delta s - s) + (s_j - s)(s - s_j + 3\Delta s)^2, & \\ \qquad s_j - 3\Delta s \leq s < s_j - 2\Delta s, & \\ (s - s_j + 4\Delta s)(s_j - \Delta s - s)^2 + (s_j - s)(s - s_j + 3\Delta s)(s_j - \Delta s - s) + (s_j - s)^2(s - s_j + 2\Delta s), & \\ \qquad s_j - 2\Delta s \leq s < s_j - \Delta s, & \\ (s_j - s)^3, & s_j - \Delta s \leq s < s_j, \\ 0, & s < s_j - 4\Delta s, \quad s_j \leq s. \end{cases}$$